BMC Cancer

RESEARCH

Open Access

# PLAAT2 facilitates the development of pancreatic cancer and serves as a predictor of resistance to chemotherapy

Qiyang Chen[1,3†], Ting Liang[2,3†], Chenhao Wu[1,3†], Jingjing Lu[3], Xiaohong Li[3], Jian Wan[1], Yuhua Lu[1*] and Qingsong Guo[1*]

## Abstract

**Background** Pancreatic cancer (PC) remains one of the deadliest human malignancies, and reliable biomarkers for prognosis and therapeutic stratification are still lacking. PLAAT2 (phospholipase A and acyltransferase 2), an enzyme linked to lipid metabolism, has been implicated in metabolic regulation, but its role in PC is not fully defined.

**Methods** Transcriptomic profiles from TCGA-PAAD and independent GEO datasets, together with the corresponding clinical annotations, were analysed to clarify the prognostic relevance and biological roles of PLAAT2. Functional enrichment, immune-cell infiltration, mutational profiles and predicted drug responses were analyzed, and a PLAAT2-related prognostic signature was generated by LASSO–Cox analysis and validated in external GEO datasets. In parallel, PLAAT2 expression was examined in paired PC tissues and matched non-cancerous counterparts by immunohistochemistry (IHC) and quantitative RT-PCR. The effects of PLAAT2 silencing on proliferation, migration, invasion and oxaliplatin sensitivity were evaluated in MiaPaCa-2 and CFPAC-1 cells.

**Results** PLAAT2 levels were substantially higher in PC specimens, and tumours with high PLAAT2 expression tended to exhibit more advanced grade and stage together with poorer survival. High PLAAT2 expression was enriched in lipid-metabolic pathways and linked to an immune-dysregulated microenvironment characterized by reduced $CD8^+$ T-cell infiltration and increased macrophages. The PLAAT2-high cohort also exhibited a higher frequency of somatic mutations, particularly in KRAS and TP53. An 11-gene PLAAT2-related signature stratified patients into distinct risk groups; high-risk patients showed significantly worse survival and lower predicted sensitivity to irinotecan, olaparib and oxaliplatin, and these findings were consistently validated in independent GEO cohorts. In an institutional cohort of 15 paired clinical samples, IHC and qRT-PCR confirmed higher PLAAT2 expression in tumor tissues than in adjacent non-tumor tissues. Functionally, PLAAT2 knockdown in MiaPaCa-2 and CFPAC-1 cells suppressed cell growth,

†Qiyang Chen, Ting Liang and Chenhao Wu contributed equally to this work.

*Correspondence:
Yuhua Lu
lyh76@126.com
Qingsong Guo
ntgglj@163.com

Full list of author information is available at the end of the article

© The Author(s) 2025. **Open Access** This article is licensed under a Creative Commons Attribution-NonCommercial-NoDerivatives 4.0 International License, which permits any non-commercial use, sharing, distribution and reproduction in any medium or format, as long as you give appropriate credit to the original author(s) and the source, provide a link to the Creative Commons licence, and indicate if you modified the licensed material. You do not have permission under this licence to share adapted material derived from this article or parts of it. The images or other third party material in this article are included in the article's Creative Commons licence, unless indicated otherwise in a credit line to the material. If material is not included in the article's Creative Commons licence and your intended use is not permitted by statutory regulation or exceeds the permitted use, you will need to obtain permission directly from the copyright holder. To view a copy of this licence, visit http://creativecommons.org/licenses/by-nc-nd/4.0/.

migration and invasion and significantly enhanced the growth-inhibitory effect of oxaliplatin, accompanied by reduced $IC_{50}$ values.

**Conclusion** Collectively, these data support an oncogenic role of PLAAT2 in PC and indicate that PLAAT2 and its associated transcriptional signature may serve as potential biomarkers of prognosis and chemotherapeutic response, as well as candidate targets for precision therapy in PC.

**Keywords** Pancreatic cancer, PLAAT2, Prognostic marker, Drug resistance, Proliferation, Invasion

## Introduction

Worldwide, PC persists as a lethal malignancy with a dismal prognosis. characterized by delayed detection, aggressive clinical course, and restricted therapeutic choices [1, 2]. Although substantial progress has been achieved in surgery and systemic treatments, the five-year survival probability of PC patients is still under 10%, and ranks seventh among the causes of cancer death worldwide [3]. Although molecular markers including KRAS, TP53, and SMAD4 have advanced insights into PC biology, they remain insufficient to account for the marked heterogeneity and therapeutic resistance of this disease [4–7]. Therefore, it is imperative to discover new markers that can refine risk stratification and direct individualized therapeutic approaches.

Reprogramming of metabolism is a defining feature of cancer, facilitating cellular adaptation to nutrient-limited microenvironments, remodel membrane structures, and sustain malignant progression [8–10]. Lipid metabolism plays a central role in membrane assembly, energy homeostasis, and signal transduction, and is increasingly acknowledged as an essential contributor to tumor invasion and therapeutic resistance [11–14]. Several lipid-metabolizing enzymes, such as acyl-CoA synthetases and phospholipases, have been associated with the development of PC. Nevertheless, the functional roles of numerous lipid regulatory factors are still not well elucidated.

Phospholipase A and acyltransferase 2 (PLAAT2, also known as HRAS-like suppressor 2,HRASLS2),belonging to the PLAAT enzyme family, is involved in phospholipid remodeling and displays acyltransferase activity [15–18]. Previous studies have indicated that PLAAT2 contributes to lipid homeostasis, oxidative stress response, and intracellular signaling. Dysregulation of PLAAT family members has been linked to inflammatory diseases and various cancers, yet the biological and clinical significance of PLAAT2 in PC has not been systematically investigated [18]. Recently, a study in pancreatic ductal adenocarcinoma reported that HRASLS2/PLAAT2 is up-regulated in tumour tissues and promotes tumour growth by modulating ASPH-related metabolic signalling, supporting an oncogenic role of PLAAT2 in PC [19]. Nevertheless, the broader clinical and biological landscape associated with PLAAT2 expression—particularly its relationships with the tumour immune microenvironment, mutational profiles and chemotherapeutic response—has not been systematically investigated [20–22].

In this study, we integrated multi-omics bioinformatic analyses with experimental validation to comprehensively evaluate the prognostic value, biological functions and immune associations of PLAAT2 in PC. Clinicopathologic annotations and follow-up information from the TCGA and GEO datasets were integrated to examine how PLAAT2 expression relates to patient prognosis, and we subsequently characterised PLAAT2-associated signalling pathways, immune landscapes, mutational features and inferred chemotherapeutic responses. To improve prognostic accuracy, we developed and validated a PLAAT2-associated multigene signature. In addition, using paired clinical specimens and in-vitro assays, we confirmed the overexpression of PLAAT2 in PC tissues and investigated its effects on proliferation, migration, invasion and oxaliplatin sensitivity in PC cell lines. Collectively, our work complements and extends previous findings on PLAAT2 by providing an integrated view of its clinical relevance and functional roles in PC, and highlights PLAAT2 and its related transcriptional programme as potential prognostic biomarkers and therapeutic targets.

## Materials and methods

### Clinical tissue specimens

Fifteen pairs of PC tissues and their matched adjacent non-tumor counterparts were obtained from patients undergoing surgical treatment in the Department of Hepatobiliary and Pancreatic Surgery, Affiliated Hospital of Nantong University, during January–November 2025. None of these individuals had received preoperative chemotherapy or radiotherapy. Immediately after resection, samples were either immersed in liquid nitrogen for snap-freezing or preserved in 4% paraformaldehyde for downstream analyses. The clinicopathological data of the patients—including age-ranges, pathological stage, Ki-67 index, and AJCC (8th edition) classification—are summarized in Table 1. Written informed consent was secured from all subjects, and the protocol was reviewed and approved by the Ethics Committee of the Affiliated Hospital of Nantong University (Approval No. 2025-K195).

**Table 1** Clinicopathological characteristics of PC patients

| Characteristic | n (%) |
|---|---|
| Age | |
| <60 | 5(33.33%) |
| ≥60 | 10(66.67%) |
| Gender | |
| Male | 6(40.00%) |
| Female | 9(60.00%) |
| Drinking history | |
| Yes | 6(40.00%) |
| No | 9(60.00%) |
| Smoking history | |
| Yes | 6(40.00%) |
| No | 9(60.00%) |
| Tumor size (cm) | |
| <3 | 9(60.00%) |
| ≥3 | 6(40.00%) |
| Tumor location (no. [%]) | |
| Head and neck of pancreas | 9(60.00%) |
| Body and nail of pancreas | 6(40.00%) |
| Lymph node metastasis | |
| Yes | 11(73.33%) |
| No | 4(26.67%) |
| TNM stage | |
| Ⅰ / Ⅱ | 13(86.67%) |
| Ⅲ/Ⅳ | 2(13.33%) |
| CEA level (mg/L, no. [%]) | |
| <5 | 12(80.00%) |
| ≥5 | 3(20.00%) |
| CA19-9 level (v/ml) | |
| <37 | 10(66.67%) |
| ≥37 | 5(33.33%) |
| Ki-67 positivity | |
| <20% | 13(86.67%) |
| ≥20% | 2(13.33%) |

#### Immunohistochemistry (IHC)

Formalin-fixed, paraffin-embedded tumour and matched adjacent non-tumour tissues from 15 patients with PC were used for IHC staining. For morphological evaluation, adjacent sections were stained with haematoxylin and eosin (H&E) using standard protocols. H&E staining was used to confirm the pathological diagnosis and to select representative tumour and adjacent non-tumour areas for IHC assessment and imaging. Section (4 μm) were deparaffinized in xylene, rehydrated through a graded ethanol series and subjected to antigen retrieval in citrate buffer (pH 6.0) using a pressure cooker for 3 min. Endogenous peroxidase activity was blocked with 3% hydrogen peroxide for 10 min, followed by blocking with 5% normal goat serum for 30 min at room temperature. The sections were then incubated with an anti-PLAAT2 antibody (Zenbio, Cat.#161756, China; 1:500 dilution) at 4 °C overnight. After washing, slides were incubated with an HRP-conjugated secondary antibody for 30 min and visualized using 3,3′-diaminobenzidine (DAB) as chromogen. Nuclei were counterstained with haematoxylin, and the slides were dehydrated and mounted. PLAAT2 staining was evaluated using a semi-quantitative H-score system. For eachcase, the percentage of positively stained tumour cells (0–100%) and the staining intensity (0 = negative, 1 = weak, 2 = moderate, 3 = strong) were recorded. The H-score was calculated as $\Sigma$ (Pi × Ii), where Pi is the percentage of cells at each intensity and Ii is the corresponding intensity score, yielding a total score ranging from 0 to 300. All slides were independently assessed by two experienced pathologists who were blinded to the clinicopathological data, and discrepancies were resolved by joint review.

#### Cell culture

A panel of human PC cell lines (BxPC-3, CFPAC-1, SW1990, Capan-2, PANC-1 and MiaPaCa-2), together with the immortalized pancreatic ductal epithelial cell line HPDE6-C7, was used in this study. All cell lines were purchased from the Cell Bank of the Chinese Academy of Sciences (Shanghai, China) and cultured in DMEM supplemented with 10% fetal bovine serum and penicillin–streptomycin at 37 °C in a humidified incubator with 5% $CO_2$.

#### RNA extraction and quantitative real-time PCR (qRT-PCR)

Total RNA was isolated with TRIzol reagent and quantified spectrophotometrically. Reverse transcription was performed to generate cDNA, followed by qRT-PCR using SYBR Green chemistry on a real-time PCR platform. Primer sequences were synthesized commercially and are provided in Supplementary Table S1. GAPDH was used as an internal reference, and relative expression levels were determined with the 2^−ΔΔCt method [23]. All experiments were repeated independently three times.

#### Western blotting

Proteins were extracted using RIPA buffer supplemented with protease and phosphatase inhibitors, and concentrations were measured with a BCA assay. Equal protein samples were resolved by SDS-PAGE and transferred onto PVDF membranes. After blocking, membranes were incubated overnight at 4 °C with primary antibodies against PLAAT2 (1:1000, Zenbio, Cat#161756, China) and GAPDH (1:5000, Proteintech, Cat No. 10494-1-AP, China) followed by HRP-conjugated secondary antibodies. Signals were detected using an enhanced chemiluminescence system.

#### SiRNA transfection

PLAAT2-targeting and negative control siRNAs (sequences in Supplementary Table S1) were introduced

into MiaPaCa-2 and CFPAC-1 cells using a commercial transfection reagent. Knockdown efficiency was verified 48 h post-transfection by qRT-PCR and Western blot.

#### Cell proliferation assays

Cell viability was assessed using the CCK-8 method, while DNA synthesis was evaluated with an EdU incorporation assay. For the CCK-8 assay, siRNA-transfected MiaPaCa-2 and CFPAC-1 cells were seeded in 96-well plates, and absorbance at 450 nm was measured at different time points to determine viability. For the EdU assay, cells were exposed to EdU, followed by fixation, staining, and fluorescence microscopy. The proportion of EdU-positive cells was quantified from multiple random fields.

#### Cell migration and invasion assays

Cell motility was evaluated using both Transwell and wound-healing assays. For the Transwell assay, siRNA-transfected cells were seeded into chambers with or without Matrigel coating to assess migration and invasion, respectively. After incubation, cells that traversed the membrane were fixed, stained, and quantified microscopically [24]. For the wound-healing assay, a scratch was introduced into confluent monolayers, and gap closure was monitored at designated time points in serum-free medium. The percentage of wound closure was calculated to compare migratory capacity [25].

#### Cell viability assay and IC50 determination

MiaPaCa-2 and CFPAC-1 cells transfected with siNC or PLAAT2 siRNAs were seeded into 96-well plates at a density of 3 × 10^3–5 × 10^3 cells per well in complete medium. After overnight attachment, cells were exposed to increasing concentrations of oxaliplatin (0, 0.3, 1, 3, 10, 30 and 100 μM) for 72 h. Cell viability was then assessed using the CCK-8 assay (Dojindo, Japan) according to the manufacturer's instructions. Briefly, 10 μL of CCK-8 solution was added to each well and incubated for 1–2 h at 37 °C, and the absorbance at 450 nm was measured using a microplate reader. Relative cell viability was calculated as the percentage of the absorbance of treated cells over that of the untreated control.

Dose–response curves were generated, and IC50 values were calculated by nonlinear regression using a variable-slope dose–response model in GraphPad Prism 9.0(GraphPad Software, San Diego, CA, USA). For time-course proliferation assays, cells were treated with PBS or oxaliplatin at the indicated concentration, and OD values were recorded at 0, 24, 48, 72 and 96 h. Each experimental condition was measured in triplicate, and all experiments were independently repeated at least.

three times.

#### Data collection and preprocessing

The overall study workflow is illustrated in a schematic diagram (Fig. 1). mRNA expression profiles for pancreatic adenocarcinoma (PAAD) were retrieved from the TCGA-PAAD cohort, including 178 primary tumor specimens and 4 matched non-tumor controls. Raw RNA-seq counts and clinical metadata were preprocessed using R software 4.4.3. Additionally, somatic mutation data were retrieved from the same cohort, comprising 165 PC patients (166 tumor samples) with available clinical information. For validation, we included two independent datasets form the Gene Expression Omnibus (GEO) [26]: GSE62452 and GSE183795. The GSE62452 dataset comprises 64 tumor samples with available survival information and 61 adjacent non-tumor samples. The GSE183795 dataset includes 134 tumor samples with available survival information and 105 adjacent non-tumor samples. Both GEO datasets were downloaded and preprocessed via the R package "GEOquery" (v2.74.0). GPL6244 were used as platform annotation file to convert probe IDs to gene symbols.Probes lacking gene annotations or mapping ambiguously to more than one gene were removed, and for genes represented by multiple probes, the mean expression level was calculated to define the gene-level signal.

#### Differential gene expression analysis

The R package DESeq2 [27] (v1.46.0) was employed to detect differentially expressed genes (DEGs). Two comparisons were performed within the TCGA-PAAD dataset: (i) tumor versus normal samples, and (ii) high- versus low-PLAAT2 expression subgroups, classified according to the median expression value. Raw count data were normalized using the median-of-ratios approach in DESeq2, and differential expression was analyzed with a negative binomial generalized linear model coupled to Wald testing. Genes showing $|\log_2$ fold change$| > 1$ with an adjusted $P < 0.05$ were deemed significant. In addition, transcripts with very low abundance (< 10 total reads across all cases) were excluded before analysis.

#### Functional enrichment analysis

The R package 'clusterProfiler' (v4.14.6) [28, 29] was applied to perform functional enrichment analysis. We conducted (1) Gene Set Enrichment Analysis (GSEA) to explore signaling pathways showing differential regulation between PLAAT2-high and PLAAT2-low groups (classified according to median expression), and (2) functional enrichment analyses of DEGs, including Gene Ontology (GO) and Kyoto Encyclopedia of Genes and Genomes (KEGG). The results were visualized using the R package "enrichplot" (v1.26.6).

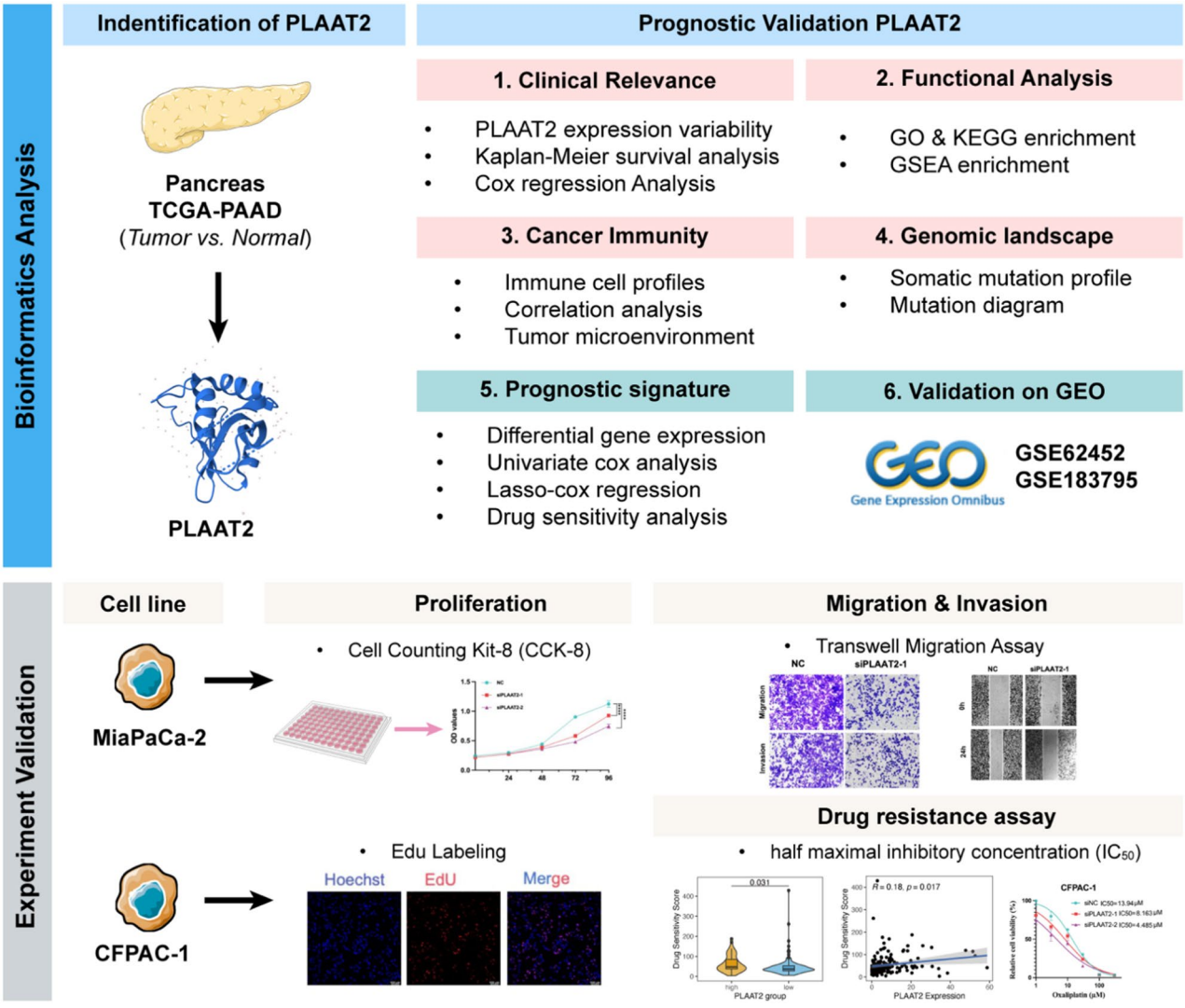



**Fig. 1** Study design flowchart. Representative experimental images (e.g., CCK-8, EdU, Transwell) are shown here as schematic thumbnails; the full datasets and detailed results are presented in Fig. 11

### Infiltration analysis of immune cells

To characterize the tumor immune microenvironment, we employed CIBERSORT [30], a widely used deconvolution algorithm that estimates the relative proportions of 22 distinct immune cell types with bulk RNA-seq data based on gene expression signatures. This method applies linear support vector regression to infer cell-type abundances from normalized gene expression profiles, leveraging a predefined leukocyte signature matrix (LM22) as a reference. We applied CIBERSORT with default parameters (100 permutations, significance threshold $P < 0.05$) to our transcriptomic datasets, filtering out samples with a CIBERSORT output P-value $\geq 0.05$ to ensure robust deconvolution results.Correlations among 22 immune cell types were evaluated using Spearman's rank correlation analysis.

### Construction of PLAAT2-derived prognostic signature

We first identified DEGs between PLAAT2-high (PLAAT2-H) and PLAAT2-low (PLAAT2-L) groups, retaining only genes with FPKM $\geq 1$ in $\geq 20\%$. Then, univariate Cox regression was applied to screen for 133 prognosis-associated candidate genes with a cutoff P-value of 0.05. The machine-learning approach, specifically, the least absolute shrinkage and selection operator (LASSO) method [31], was applied to identify key predictive variables. Implementation utilized the R package glmnet (v4.1.8),with the response type specified as "cox" and the alpha parameter fixed at 1, resulting 11 key genes. The formula for each patient's PLAAT2-derived risk score was shown below:

$$RiskScore = \sum_{i=1}^{11} \beta_i * Expression_i$$

where $\beta_i$ denotes the LASSO-Cox coefficient for each key gene; $Expression_i$ indicates normalized gene expression. Patients were divided into high- and low-risk categories using the median risk score as the cutoff for subsequent analyses.

#### Tumor microenvironment characterization

The "ESTIMATE" [32] algorithm in R was employed to assess the tumor microenvironment(v1.0.13). This algorithm infers stromal and immune cell infiltration levels in tumor tissues based on gene expression profiles. The ESTIMATE score combines stromal and immune scores to reflect overall tumor purity. Gene expression data were preprocessed and normalized before analysis. Default parameters were applied to compute stromal, immune, and ESTIMATE scores, with higher scores indicate greater immune/stromal infiltration and lower tumor purity.

#### Evaluation of drug sensitivity

Predicted responses to chemotherapeutic agents were obtained with the R package oncoPredict (v1.2) [33]. Transcriptomic profiles from tumor samples were used to estimate the half-maximal inhibitory concentration (IC50) of multiple anticancer compounds. The algorithm applies a machine-learning framework trained using data from the Genomics of Drug Sensitivity in Cancer (GDSC) database (GDSC) resource to infer drug susceptibility. Data were normalized and scaled before analysis. Default parameters were applied, and predicted $IC_{50}$ values were used to assess drug sensitivity, with lower values indicating higher drug efficacy.

#### Statistical analysis

All computational procedures were carried out in R software (v4.4.3) using relevant packages. Predictive performance was assessed using receiver operating characteristic (ROC) analysis, with the area under the curve (AUC) calculated accordingly. Survival outcomes were evaluated through Kaplan–Meier estimations combined with log-rank testing. Potential prognostic determinants were screened using univariate Cox regression and refined with LASSO-Cox modeling. Relationships between variables were evaluated via Pearson's correlation test.For experimental data, all assays were repeated independently at least three times. Results are presented as mean ± standard deviation (SD). Comparisons between two groups were performed using Student's t-test, and comparisons among multiple groups were conducted using one-way ANOVA. Statistical analyses were carried out using GraphPad Prism 9.0 (GraphPad Software, USA). A two-sided $P < 0.05$ was considered statistically significant.

## Results

#### Identification of PLAAT2 as an upregulated gene in PC

To screen for candidate biomarkers in PC, RNA-seq transcriptome data were obtained from the TCGA-PAAD cohort. After quality control, the dataset comprised 178 primary tumor specimens and 4 matched adjacent normal tissues from 178 patients.Differential expression analysis between these two groups, 503 DEGs were identified, including 220 downregulated and 283 upregulated DEGs (Fig. 2A, B). The heatmap of top 100 most significant DEGs (ranked by descending $log_2FC$) are shown in Fig. 2D. Among these, phospholipase A and acyltransferase 2 (PLAAT2) emerged as one of the significantly upregulated genes in tumor samples ($P = 0.014$, Fig. 2C). Given its marked overexpression and the paucity of studies on its functional role in PC, we selected PLAAT2 for further in-depth characterization.

#### Elevated PLAAT2 expression correlates with tumor progression and poor prognostic in PC

To assess the clinical significance of PLAAT2 in PC, we initially analyzed its expression patterns across various tumor grades and clinical stages. Results showed that PLAAT2 expression significantly increased with advancing tumor grade (Comparisons between G1 and G2, $P = 0.018$; as well as G1 and G3, $P = 0.029$), but showed no difference between G2 and G3 ($P = 0.97$) (Fig. 3A). Likewise, PLAAT2 expression was markedly higher in Stage II tumors relative to those at Stage I. ($P = 0.011$, Fig. 3B). The evidence points to PLAAT2 playing a mechanistic role in PC progression.

Next, based on the median cutoff, patients were stratified into high- (PLAAT2-H) and low-expression (PLAAT2-L) subgroups. Kaplan–Meier analysis revealed that the PLAAT2-H cohort experienced significantly worse survival compared with the PLAAT2-L cohort. ($P = 0.003$, Fig. 3C). Subsequently, We applied univariate Cox regression analysis, integrating PLAAT2 expression with key clinical and pathological variables, including sex, age, disease stage, and tumor grade. This analysis identified high PLAAT2 expression as a significant prognostic factor, along with other established clinical parameters. Notably, in a multivariate Cox regression model accounting for potential confounders, elevated PLAAT2 expression remained strongly and independently associated with unfavorable overall survival (HR = 1.71, 95% CI: 1.09–2.66, $P = 0.019$) (Table 2). Together, our data indicate that elevated PLAAT2 expression is independently associated with an unfavourable survival profile in individuals with PC.

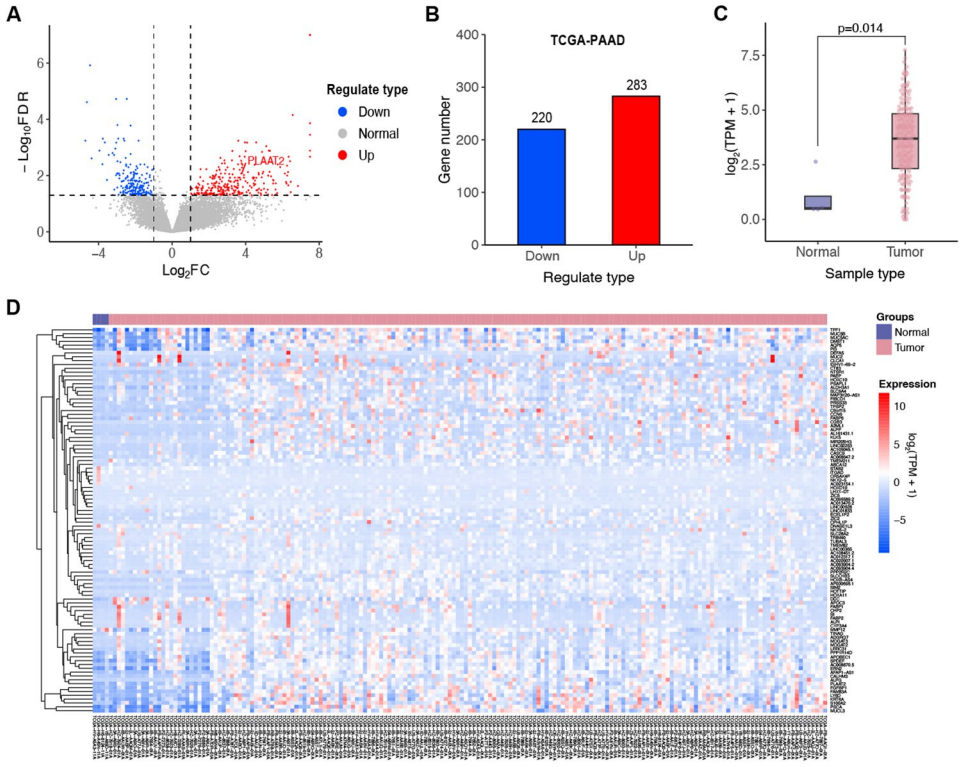



**Fig. 2** Detection of DEGs between pancreatic tumor tissues and adjacent normal samples from TCGA. **A** Volcano plot of DEGs with the criteria of $|\log_2 FC| > 1$ and adjusted P-value < 0.05. Upregulated genes are shown in red, whereas downregulated genes are depicted in blue. **B** Box plot summarizing the counts of upregulated and downregulated genes. **C** PLAAT2 expression was significantly higher in tumor specimens than in normal tissues. **D** Heatmap showing top 100 DEGs between tumor and normal samples

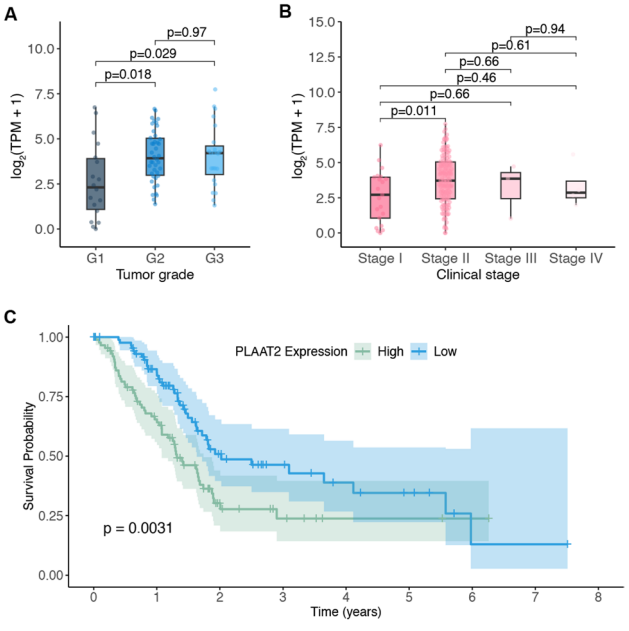



**Fig. 3** Correlations between PLAAT2 expression and clinical features of PC patients. **A** PLAAT2 expression across histological grades. **B** PLAAT2 expression across clinical stages. **C** Overall survival curves for patients grouped by PLAAT2 expression (high vs. low)

### Biological functions associated with PLAAT2 in PC

We performed differential expression analysis between the PLAAT2-H and PLAAT2-L groups and obtained 2,172 significant DEGs (425 upregulated and 1,747 downregulated) (Fig. 4A).

Gene Set Enrichment Analysis (GSEA) based on all expressed genes revealed that the PLAAT2-H subgroup was predominantly associated with metabolic pathways, including linolenic acid metabolism, ascorbate and aldarate metabolism, and folate/thiamine transport (Fig. 4B). In contrast, the PLAAT2-L subgroup showed enrichment in neural and secretory programs, such as GABAergic synapse and insulin secretion pathways (Fig. 4C).

Consistently, GO and KEGG enrichment analyses of the 2,172 DEGs indicated that these genes were mainly involved in membrane-associated biological processes, including signal transduction, secretory pathways, and lipid remodeling (Fig. 4D), in line with the known phospholipase activity of PLAAT2 and its role in membrane dynamics.

### Immunological implications of PLAAT2 in PC

To characterize the immune landscape of PC, the CIBERSORT algorithm was employed to estimate the relative abundance of 22 immune cell types in each TCGA-PAAD sample. We then compared the infiltration profiles

**Table 2** Cox regression (univariate and multivariate) analysis of PLAAT2 expression (Low vs. High) with overall survival, adjusted for clinical covariates in TCGA-PPAD

| Characteristics | Univariate analysis | | Multivariate analysis | |
|---|---|---|---|---|
| | Hazard ratio (95%) | *p* value | Hazard ratio (95%) | *p* value |
| Gender | | | | |
| Male | | | | |
| Female | 1.21 (0.81–1.83) | 0.350 | 1.29 (0.84–1.97) | 0.242 |
| Age | | | | |
| < 61 | | | | |
| 61–71 | 1.38 (0.83–2.29) | 0.209 | 1.56 (0.93–2.64) | 0.094 |
| 71–88 | 1.92 (1.16–3.20) | **0.012** | 1.86 (1.11–3.12) | **0.019** |
| Clinical Stage | | | | |
| I | | | | |
| II | 2.35 (1.08–5.12) | **0.032** | 2.36 (1.01–5.52) | **0.049** |
| III | 1.26 (0.15–10.32) | 0.829 | 1.13 (0.13–9.58) | 0.909 |
| IV | 2.14 (0.44–10.43) | 0.348 | 2.37 (0.46–12.21) | 0.303 |
| Tumor grade | | | | |
| G1 | | | | |
| G2 | 1.99 (1.03–3.86) | **0.042** | 1.25 (0.63–2.50) | 0.524 |
| G3 | 2.62 (1.30–5.27) | **0.007** | 1.51 (0.72–3.17) | 0.277 |
| G4 | 1.67 (0.21–13.1) | 0.623 | 1.24 (0.15–9.93) | 0.842 |
| PLAAT2 | | | | |
| Low | | | | |
| High | 1.86 (1.23–2.81) | **0.004** | 1.71 (1.09–2.66) | **0.019** |

Bold figures indicate $P < 0.05$ as statistically significant

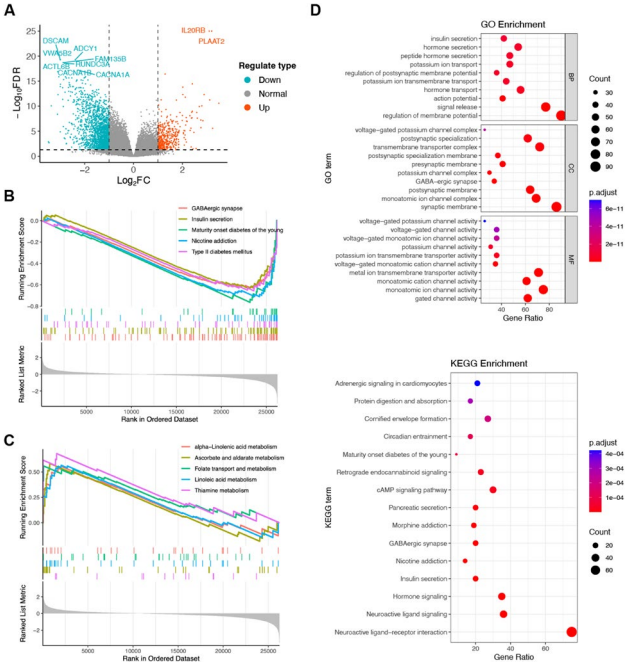



**Fig. 4** Functional annotation of differentially expressed genes (DEGs) between high- and low-PLAAT2 groups. **A** Volcano plot showing DEGs identified under the cutoff |log2FC| > 1 and adjusted $P < 0.05$. Genes with increased expression are highlighted in orange, whereas those reduced are marked in cyan. **B** GSEA illustrating pathways predominantly enriched in the low PLAAT2 subgroup. **C** GSEA illustrating pathways predominantly enriched in the high PLAAT2 subgroup. **D** The ten most significantly enriched GO terms, categorized by Biological Process (BP), Cellular Component (CC), and Molecular Function (MF). **E** The top fifteen KEGG pathways with significant enrichment

between the PLAAT2-H and PLAAT2-L groups, which showed distinct immune cell compositions (Fig. 5A, B).

We further examined the relationships among tumor-infiltrating immune cells within each subgroup. Correlation heatmaps for the PLAAT2-L and PLAAT2-H groups (Fig. 5C, D) revealed weak-to-moderate correlations between most immune subsets. Notably, $CD8^+$ T cells consistently exhibited negative correlations with M0 macrophages (high-PLAAT2: $r = -0.49$; low-PLAAT2: $r = -0.53$), whereas naïve $CD4^+$ T cells showed positive correlations with memory B cells (high-PLAAT2: $r = 0.62$; low-PLAAT2: $r = 0.52$).

Differential infiltration analysis further demonstrated that, in the PLAAT2-H group, naïve B cells, $CD8^+$ T cells, activated memory $CD4^+$ T cells, and monocytes were markedly reduced, whereas memory B cells as well as M0 and M1 macrophages were significantly enriched compared with the PLAAT2-L group (Fig. 5E). These findings suggest that high PLAAT2 expression is associated with an immunosuppressive tumor microenvironment.

### Mutation landscape comparison between PLAAT2-H and PLAAT2-L groups

Our genomic analysis revealed that 98.2% (162/165) of PC patients harbored somatic mutations. Notably, we observed a striking disparity in mutation burden between the PLAAT2-H and PLAAT2-L groups, with the former exhibiting 21,432 mutations compared to only 3076 in the latter. Fig. 6A, B illustrated the five most frequently mutated genes across all samples, i.e., KRAS (77% in PLAAT2-H and 43% in

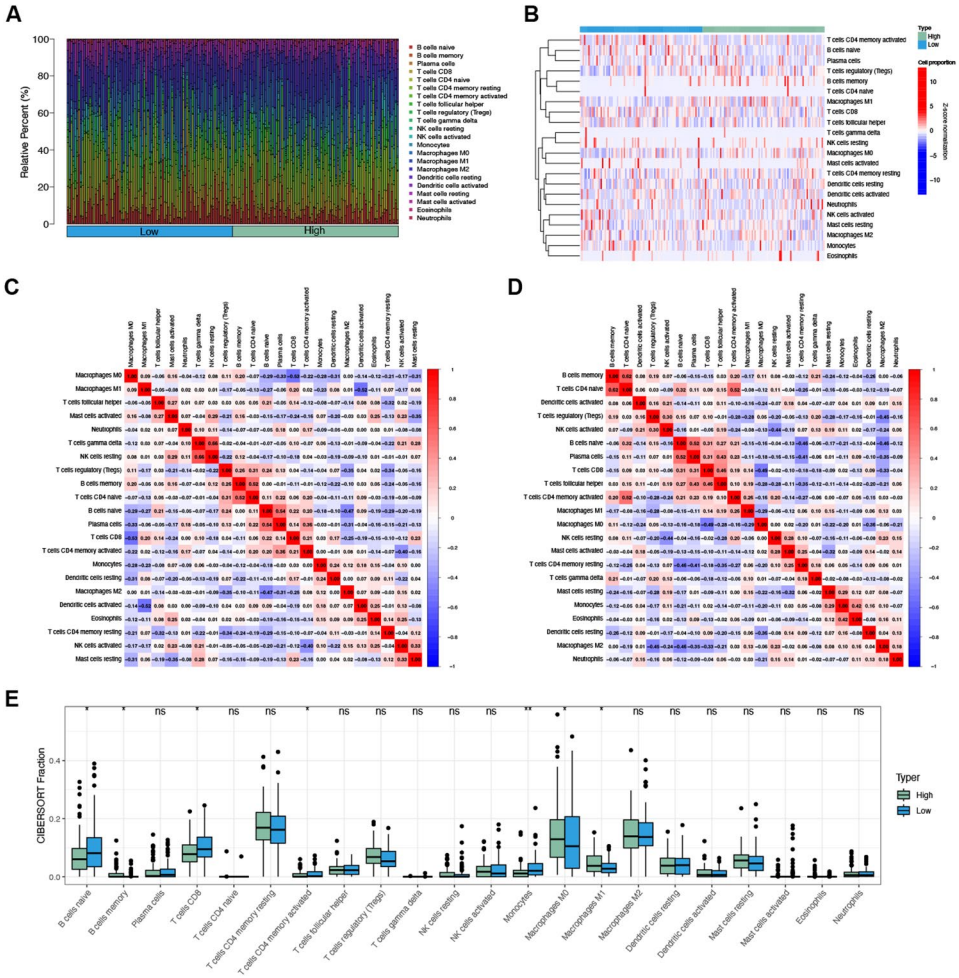



**Fig. 5** Immunological landscape comparison between high- and low-PLAAT2 groups. **A** Relative proportions of 22 immune cell types in each PC sample, estimated using the CIBERSORT algorithm. **B** Heatmap of the immune cells abundance in each PC patients. **C** Correlation evaluation between different immune cell types in low-PLAAT expression group. **D** Correlation evaluation between different immune cell types in high-PLAAT expression group. **E** Comparative analysis of immune cell fractions in tumors with high versus low PLAAT2 expression

PLAAT2-L), TP53(71% in PLAAT2-H and 45% in PLAAT2-L), SMAD4 (25% in PLAAT2-H and 18% in PLAAT2-L), CDKN2A (24% in PLAAT2-H and 11% in PLAAT2-L) and TTN (14% in PLAAT2-H and 12% in PLAAT2-L). Among the most frequently altered genes, mutations in KRAS, TP53, and CDKN2A were markedly more common in the PLAAT2-H cohort than in the PLAAT2-L group (Fig. 6C). We subsequently characterized the mutation spectra of these three genes (Fig. 6D): TP53 displayed the most diverse mutation profile, with numerous mutation sites distributed across the gene. While KRAS mutations in both groups occurred at identical genomic positions, the PLAAT2-H group exhibited a broader spectrum of mutation types at these loci. CDKN2A demonstrated fundamentally distinct mutation patterns between the two groups.

### Prognostic evaluation of PLAAT2-derived signature in PC

Through univariate Cox regression analysis of DEGs between PLAAT2-H and PLAAT2-L groups, we initially identified 133 survival-related prognostic genes ($P<0.05$). To refine this gene set and prevent overfitting, we subsequently performed LASSO regression analysis, which yielded 11 optimally prognostic genes: TEKT2, GALNT16, NACAD, HMGA2, RIC3, ARNT2, SLC16A11, CA8, TMEM139, NT5M, and ZNF488. The hazard ratios for these selected genes are presented in Fig. 7A. Using these 11 selected genes, we developed a prognostic risk model via multivariate Cox regression. For each patient, the RiskScore was derived using the formula: RiskScore = (-0.0185 × TEKT2 expression) + (-0.0933 × GALNT16 expression) + (-0.0057 × NACAD expression) + (0.1175 × HMGA2 expression) + (-0.0169 × RIC3 expression) + (-0.01711 × ARNT2 expression) + (-0.0881 × SLC16A11 expression) + (-0.0704 × CA8 expression) + (0.1064 × TMEM139 expression) + (-0.0518 × NT5M expression) + (-0.0069 × ZNF488 expression). Using the median RiskScore as a cutoff, PC patients were stratified into high- and low-risk groups. A

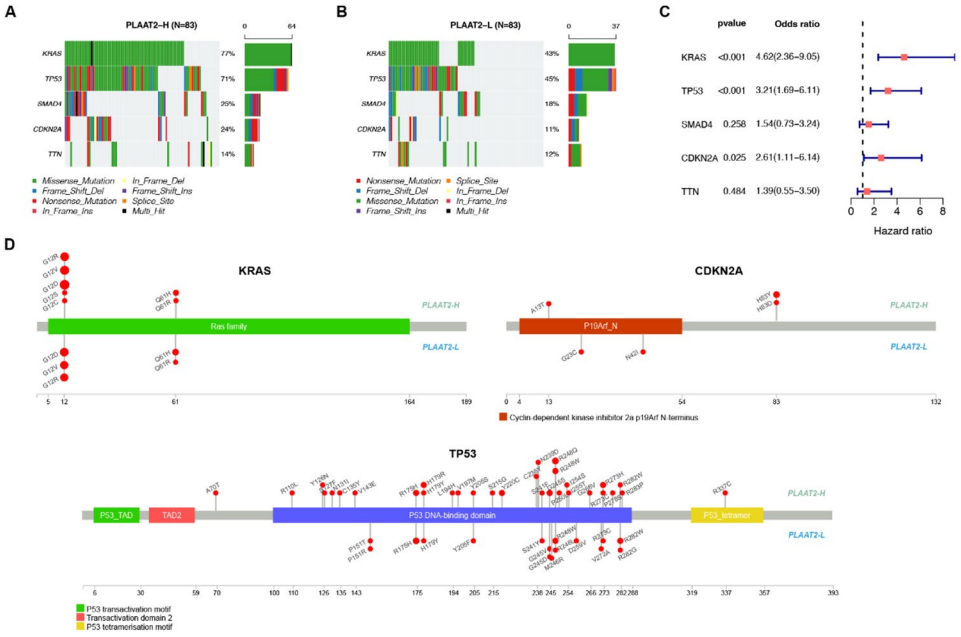



**Fig. 6** Association between PLAAT2 expression and mutation profile in the TCGA-PAAD dataset. **A** Five most frequently mutated genes in the PLAAT2-H subgroup. **B** Five most frequently mutated genes in the PLAAT2-L subgroup. **C** Forest plot summarizing the top five mutated genes in both groups, where an odds ratio > 1 denotes a higher mutation rate in the PLAAT2-H group. **D** Lollipop plot of somatic mutation for KRAS, CDKN2A, and TP53, respectively

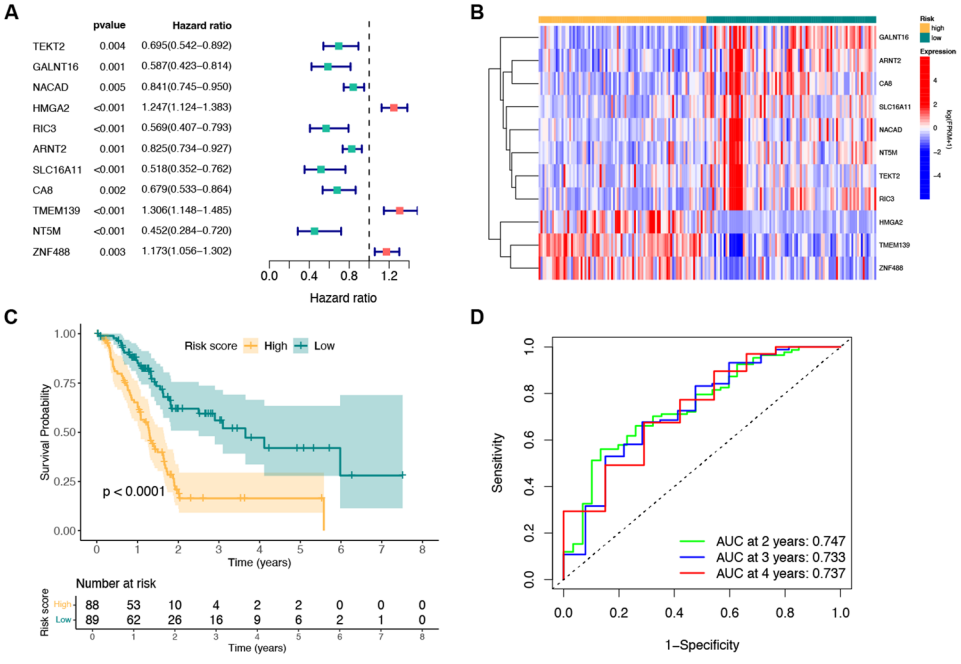



**Fig. 7** Construction of an PLAAT2-derived signature for PC prognosis. **A** Forest plot showing hazard ratios for the 11 prognostic genes included in the signature, where values > 1 denote elevated risk linked to unfavorable outcomes. **B** Heatmap illustrating the expression patterns of the 11 genes in high- and low-risk subgroups of the TCGA-PAAD cohort. **C** Overall survival curves comparing patients stratified by risk level. **D** ROC analyses for 2-, 3-, and 4-year OS prediction based on the PLAAT2-related risk score

heatmap illustrates the expression patterns of the 11-gene signature between these two categories (Fig. 7B).

Survival analysis demonstrated that patients in the low-risk group exhibited significantly longer overall survival compared with those in the high-risk group ($P < 0.0001$), confirming the prognostic value of this stratification model (Fig. 7C). To further assess predictive performance, ROC analysis was conducted, yielding AUCs of 0.747, 0.733, and 0.737 for 2-, 3-, and 4-year overall survival, respectively (Fig. 7D), indicating stable prognostic accuracy across different time points. Furthermore, when compared with conventional clinicopathologic factors, including T, N, M stage, clinical stage and histologic grade, the PLAAT2-derived risk score achieved higher time-dependent AUCs for overall survival, suggesting added prognostic value beyond established staging systems (Table S2).

### PLAAT2-derived risk stratification reveals distinct tumor microenvironment and drug sensitivity in PC

We utilized the ESTIMATE method to systematically assess tumor microenvironment (TME) features for every PC patient.This computational approach generated three distinct biological scores for every case: Stromal Score (indicating stromal cell infiltration), Immune Score (reflecting immune cell infiltration), and ESTIMATE Score (representing the overall tumor purity). Comparative analysis demonstrated significant variations in these microenvironmental parameters across the high- and low-risk groups (Fig. 8A). In particular, Immune Scores were markedly elevated in the low-risk group relative to the high-risk group ($P = 0.001$). This pattern was observed across all three scoring systems, indicating that patients with lower risk values exhibit more pronounced immune infiltration in the tumor microenvironment. To further assess the link between the PLAAT2-based risk score and therapeutic response, the "oncoPredict" package was utilized to predict drug sensitivity profiles for all patients. Correlation analysis identified significant associations between the risk score and drug responsiveness (Fig. 8B). Of note, three chemotherapeutic agents—Iriniotecan, Olaparib, and Oxaliplatin—displayed significantly higher predicted sensitivity scores in the high-risk subgroup, indicating stronger resistance compared with the low-risk group. These findings suggest that patients with higher risk scores are less responsive to standard therapeutic regimens.

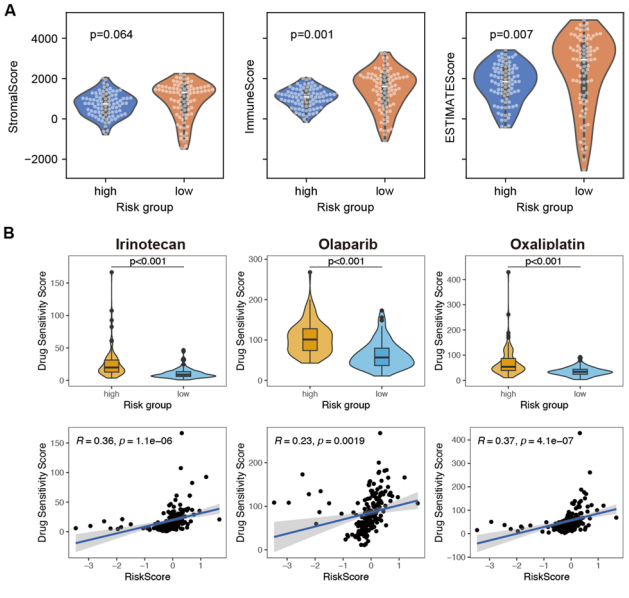



**Fig. 8** PLAAT2 risk stratification reveals distinct TME profiles and drug sensitivity in PC. **A** Analysis of stromal, immune, and composite scores calculated by ESTIMATE, contrasted between high- and low-risk subgroups. **B** Violin plots illustrating predicted responses to Irinotecan, Olaparib, and Oxaliplatin, together with their association with risk scores in the TCGA-PAAD dataset

### Validation of PLAAT2-derived prognostic signature on GEO datasets

To assess the prognostic significance and broader applicability of the PLAAT2-based risk model, we validated it in two independent GEO PC cohorts: GSE62452 ($n = 65$) and GSE183795 ($n = 134$). Risk scores were computed for each patient using the established formula and subsequently divided into high- and low-risk categories according to the median cutoff. Kaplan–Meier curves in both datasets showed that the high-risk subgroup exhibited significantly poorer survival than the low-risk subgroup (Fig. 9A, B). These consistent findings confirm the robust prognostic accuracy of the PLAAT2-derived signature and its applicability to diverse PC patient populations.

### PLAAT2 exhibits increased expression in PC tissues and their corresponding cell lines

To validate the clinical significance of PLAAT2, we first measured its expression in paired tumor and adjacent non-tumor tissues collected from 15 PC patients at our institution. A representative H&E and IHC staining pattern is shown in Fig. 10A, in which tumor tissues exhibited substantially stronger PLAAT2 staining than matched adjacent non-tumor samples. Semi-quantitative H-score analysis confirmed that PLAAT2 protein levels were significantly higher in tumor tissues than in adjacent tissues (***$P < 0.001$; Fig. 10B). Consistently, qRT-PCR analysis of the same 15 pairs further verified that PLAAT2 mRNA expression was markedly upregulated in tumor tissues (**$P < 0.01$; Fig. 10C). These findings align with our computational analyses and suggest that PLAAT2 may function as an oncogenic driver in PC.

Next, we examined PLAAT2 expression across six widely used PC cell lines (BxPC-3, CFPAC-1, SW1990, Capan-2, Panc-1, and MiaPaCa-2) in comparison with

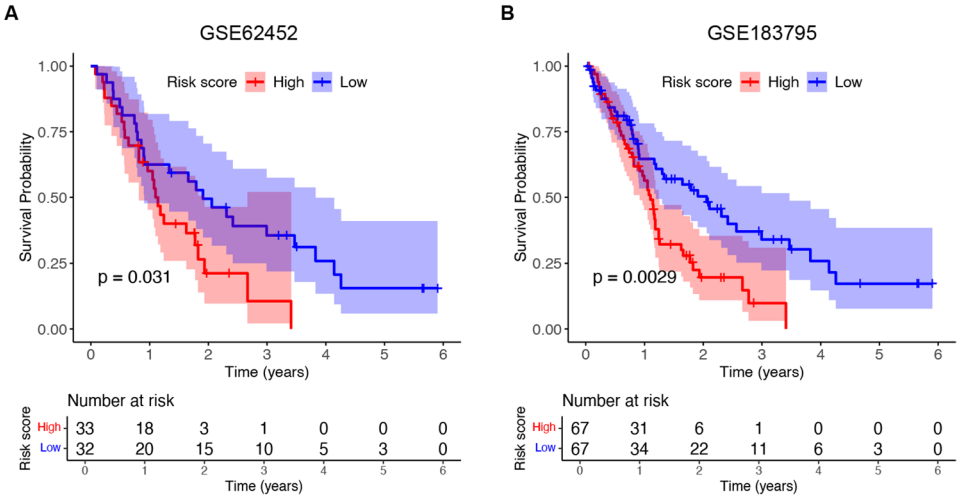



**Fig. 9** Prognostic validation of the PLAAT2-derived signature in independent GEO datasets. **A** K-M survival analyses showing overall survival differences in the GSE62452 dataset for high- versus low-risk patients. **B** Survival curves from the GSE183795 cohort illustrating OS disparities between the two risk groups

the immortalized normal pancreatic ductal epithelial cell line HPDE6-C7. Western blotting showed that PLAAT2 levels were significantly elevated in BxPC-3, MiaPaCa-2, and CFPAC-1 cells relative to HPDE6-C7 (Fig. 10D). For the downstream functional experiments, we utilized MiaPaCa-2 and CFPAC-1 cell models.

### Silencing PLAAT2 inhibits the proliferative capacity of PC cells

To explore the role of PLAAT2 in driving PC progression, we used RNA interference with siRNAs to knock down PLAAT2 in MiaPaCa-2 as well as CFPAC-1 cells. Both Western blot and qRT-PCR results demonstrated efficient silencing of PLAAT2, with siPLAAT2-2 exhibiting the strongest knockdown efficiency (Fig. 10E-H).

Functional assays demonstrated that PLAAT2 knockdown significantly impaired PC cell proliferation. CCK-8 assays showed a marked reduction in cell viability following PLAAT2 silencing compared with negative control groups ($P<0.0001$; Fig. 11A-B). Similarly, EdU incorporation assays revealed decreased DNA synthesis in siPLAAT2-transfected cells, thereby reinforcing that PLAAT2 depletion exerts a suppressive effect on PC cell proliferation (Fig. 11C-F).

### Silencing PLAAT2 reduces the migratory and invasive abilities of PC cells

To further delineate its role in modulating cell motility in PC, we performed Transwell and Matrigel invasion assays. The results showed that PLAAT2 silencing markedly diminished the migration and invasion abilities of MiaPaCa-2 and CFPAC-1 cells relative to the controls ($P<0.05$; Fig. 11G-H, K-L). Consistently, wound-healing assays revealed a marked delay in closure rate in siPLAAT2-transfected cells, indicating impaired migratory ability (Fig. 11I-J, M-N).

Taken together, these experiments demonstrate that PLAAT2 is upregulated in PC tissues and cell lines, and its silencing effectively inhibits cell proliferation, migration, and invasion. These results are consistent with the bioinformatics analyses, supporting the oncogenic role of PLAAT2 in PC progression.

### PLAAT2 expression is associated with reduced chemosensitivity and its silencing increases the response to oxaliplatin in PC cells

Given the clinical use of several cytotoxic and targeted agents in PC, we next examined the relationship between PLAAT2 expression and predicted sensitivity to commonly used drugs. Using the TCGA-PAAD cohort and the oncoPredict algorithm, patients were divided into PLAAT2-high and PLAAT2-low groups, and drug response scores were inferred for irinotecan, olaparib and oxaliplatin. In all three cases, tumors with low PLAAT2 expression showed significantly more favourable predicted responses than those with high PLAAT2 expression (Fig. 12A, upper panels). Consistently, PLAAT2 mRNA levels were positively correlated with the predicted drug response scores for irinotecan, olaparib and oxaliplatin ($R\approx0.18$–$0.26$, all $P<0.05$; Fig. 12A, lower panels), suggesting that upregulation of PLAAT2 may be linked to a less chemosensitive phenotype.

To functionally validate these predictions, we investigated the effect of PLAAT2 knockdown on oxaliplatin response in MiaPaCa-2 and CFPAC-1 cells. CCK-8–based dose–response assays showed that silencing PLAAT2 shifted the oxaliplatin curves leftwards in both cell lines, with a marked reduction in $IC_{50}$ values

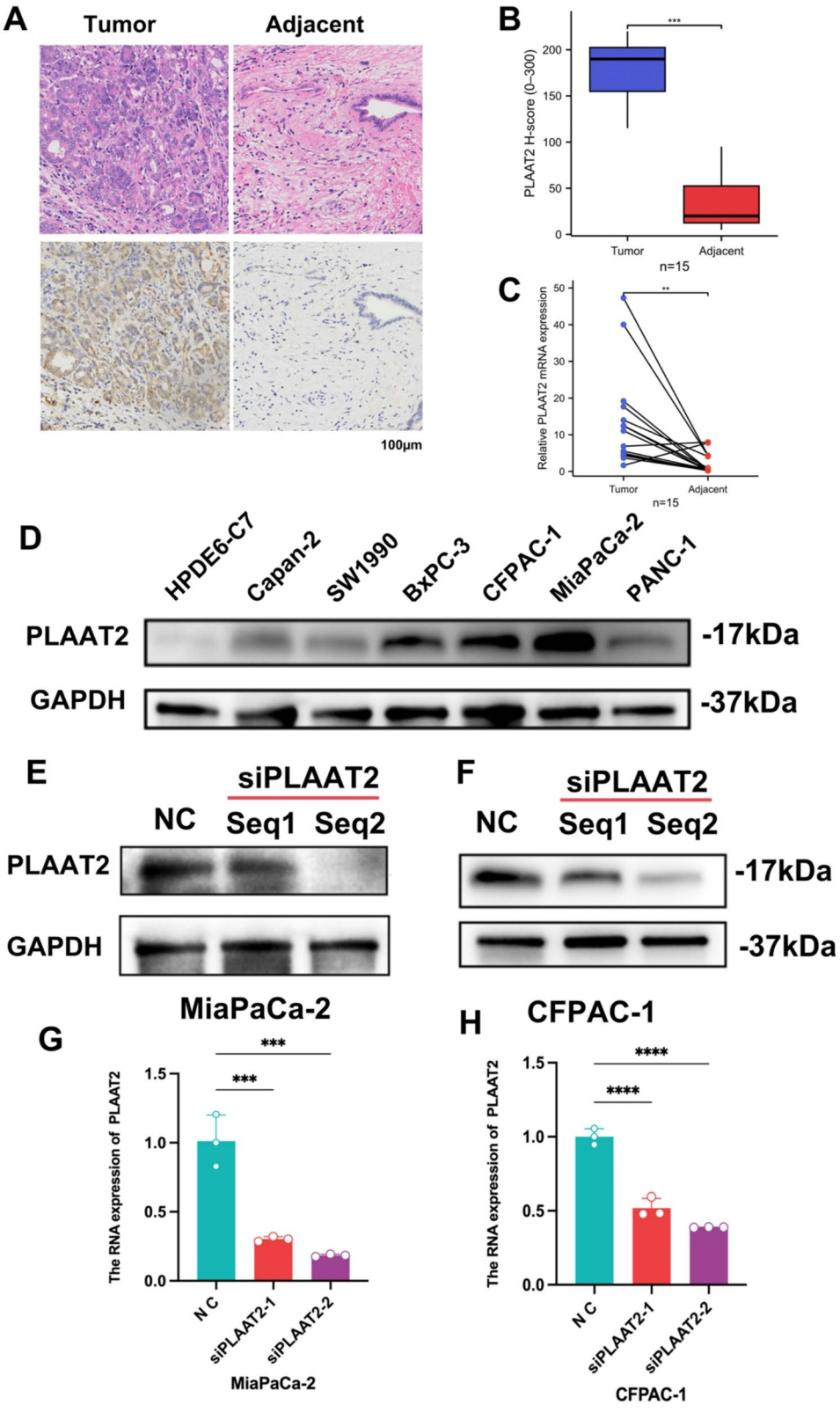



**Fig. 10** (See legend on next page.)

(See figure on previous page.)

**Fig. 10** PLAAT2 expression is elevated in PC tissues and cell lines. **A** Representative H&E and immunohistochemical staining of PLAAT2 in primary pancreatic cancer (Tumor) and matched adjacent non-tumor tissue (Adjacent). Scale bar, 100 μm. **B** Quantitative comparison of PLAAT2 protein expression between primary pancreatic cancer (Tumor) and matched adjacent non-tumor tissues. (Adjacent) in 15 patients. PLAAT2 staining was evaluated using the H-score system (0–300). Boxes indicate the interquartile range, horizontal lines represent the median, and whiskers show the minimum and maximum values. Statistical significance was determined by the Wilcoxon signed-rank test (***$P < 0.001$). **C** qRT-PCR quantification of PLAAT2 mRNA levels in paired tumor and adjacent non-tumor tissues ($n = 15$). Results are shown as mean ± SD; $P < 0.01$. **D** Western blot assessment of PLAAT2 protein expression in seven PC cell lines (BxPC-3, CFPAC-1, SW1990, Capan-2, Panc-1, and MiaPaCa-2) and the normal pancreatic ductal epithelial line HPDE6-C7. **E**-**H** Validation of siRNA-mediated silencing efficiency in MiaPaCa-2 and CFPAC-1 cells using qRT-PCR and Western blot. Among them, siPLAAT2-2 achieved the most effective knockdown and was selected for subsequent assays. (***$P < 0.001$,****$P < 0.0001$)

compared with siNC-transfected cells (MiaPaCa-2: from 10.68 μM to 5.85 μM and 3.55 μM for siPLAAT2-1 and siPLAAT2-2, respectively; CFPAC-1: from 13.94 μM to 8.16 μM and 4.49 μM; Fig. 12B, C). Time-course proliferation assays further demonstrated that PLAAT2 knockdown significantly reinforced the growth-inhibitory effect of oxaliplatin: while PLAAT2 silencing alone had only a modest impact on cell proliferation, the combination of siPLAAT2-2 with oxaliplatin produced the lowest OD values at 72–96 h in both MiaPaCa-2 and CFPAC-1 cells (Fig. 12D, E), indicating that depletion of PLAAT2 sensitizes PC cells to oxaliplatin.

## Discussion

PC is distinguished by its aggressive biology, pronounced heterogeneity and limited therapeutic options [1, 2], highlighting the urgent requirement for novel prognostic markers and actionable treatment avenues. In this work, we combined multi-omics bioinformatic analyses with experimental validation to characterize the clinical and biological relevance of PLAAT2 in PC. Across public datasets, PLAAT2 expression was consistently upregulated in tumour tissues and associated with adverse clinicopathological features and poorer overall survival, and these findings were corroborated in a small institutional cohort. Together with our in vitro data, these observations support a tumour-promoting role of PLAAT2 in PC.

PLAAT2 belongs to the PLAAT family and participates in phospholipid remodelling and acyltransferase reactions, linking it tightly to lipid metabolism [15–18]. We found that PLAAT2-high tumours were enriched in lipid-related pathways and membrane-associated biological processes, which is consistent with the established biochemical properties of PLAAT2 and the broader concept that metabolic rewiring is integral to pancreatic tumour progression [8, 11–13, 15–17]. Recent work in PC has reported that HRASLS2/PLAAT2 is upregulated in pancreatic ductal adenocarcinoma and promotes tumour growth through ASPH-dependent metabolic signalling [19], providing mechanistic evidence that PLAAT2 can act as an oncogenic factor in this disease. Our results complement and extend these findings by placing PLAAT2 within a wider molecular context that encompasses not only metabolic pathways but also immune-cell composition, mutational profiles and chemotherapeutic response.

One of the notable observations in our study is the association between high PLAAT2 expression and an altered tumour immune microenvironment. PLAAT2-high tumours exhibited reduced infiltration of $CD8^+$ T cells and activated memory $CD4^+$ T cells, accompanied by increased M0/M1 macrophages and memory B cells [20, 22]. At first glance, the enrichment of M1 macrophages may appear inconsistent with an immunosuppressive milieu, because M1 macrophages are classically regarded as pro-inflammatory cells that facilitate antigen presentation and support cytotoxic T-cell responses. However, accumulating evidence indicates that macrophage phenotypes in human cancers are highly plastic and seldom conform to a strict M1/M2 dichotomy, and that "M1-like" inflammatory macrophages in chronic tumour settings can coexist with, or even contribute to, immune dysfunction and tumour progression. In this context, the immune pattern observed in PLAAT2-high tumours – reduced $CD8^+$ T-cell infiltration together with increased macrophage infiltration – is more compatible with a state of chronic, dysfunctional inflammation than with an effective anti-tumour response. This interpretation is also in line with the enrichment of inflammatory and immunoregulatory pathways in PLAAT2-high tumours, and with previous reports that lipid metabolic rewiring can influence antigen presentation, cytokine networks and immune-cell recruitment [9, 10, 20, 22], suggesting that PLAAT2 may help shape an immune microenvironment that is inflamed yet ultimately permissive for tumour growth.

We also observed that PLAAT2-high tumours harboured a higher burden of somatic mutations, particularly in KRAS and TP53 [34]. Although our analyses cannot establish causality, this association raises the possibility that PLAAT2-driven metabolic alterations may interact with canonical oncogenic pathways and genomic instability to accelerate tumour evolution. Previous studies have shown that lipid metabolic reprogramming can modulate signalling cascades downstream of KRAS and impact DNA-damage responses [9, 10] suggesting potential mechanistic links between PLAAT2 activity, oncogenic signalling and genome maintenance. Further work that integrates lipidomic profiling with functional assays

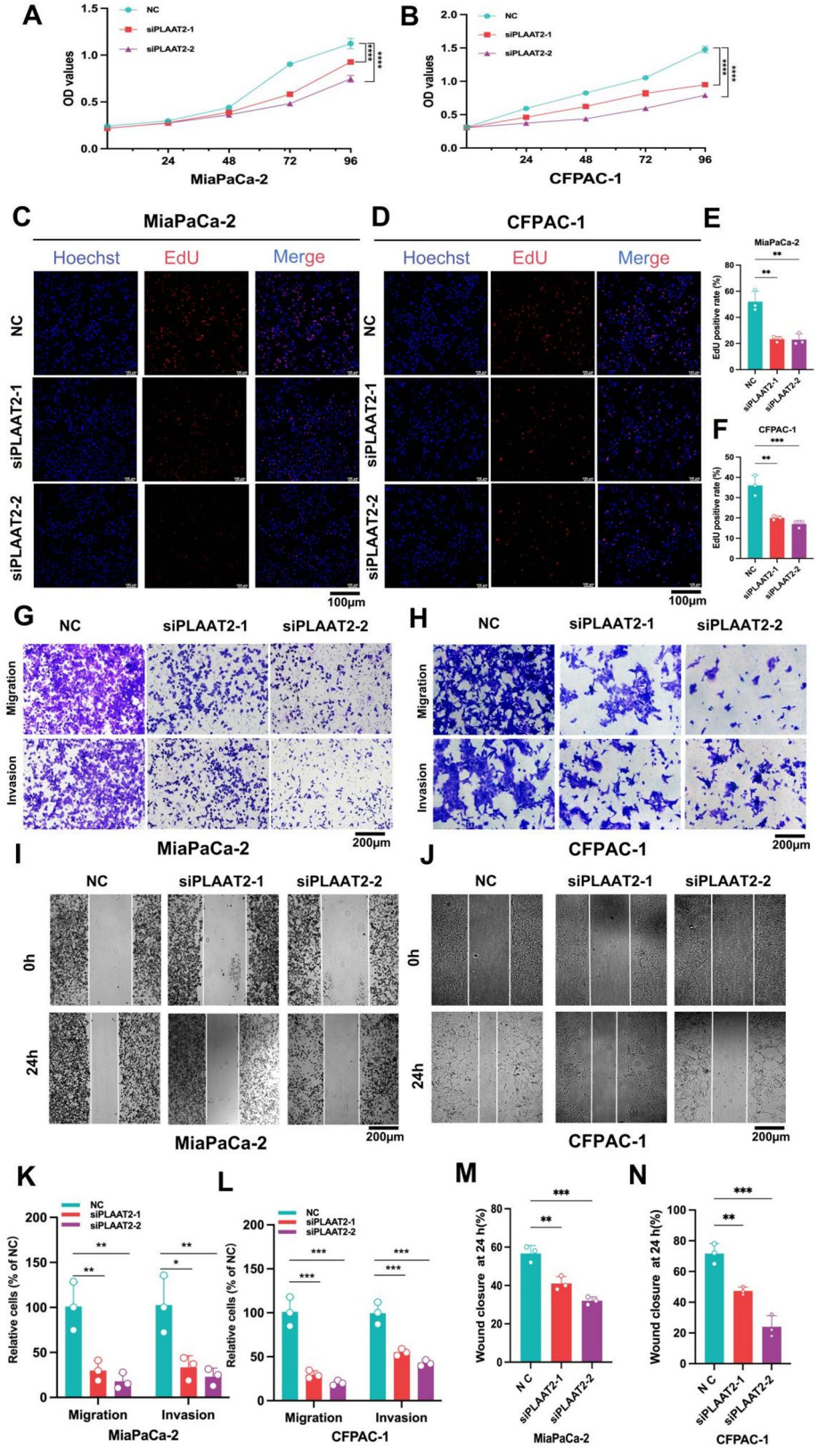



**Fig. 11** (See legend on next page.)

(See figure on previous page.)

**Fig. 11** Silencing PLAAT2 reduces the proliferative, migratory, and invasive capacities of PC cells. **A**–**B** CCK-8 assay indicating decreased viability in PLAAT2-silenced MiaPaCa-2 and CFPAC-1 cells relative to NC. **C**–**D** EdU assay showing impaired DNA synthesis following siPLAAT2 transfection. Representative images (left) and (**E**-**F**) quantitative results (right) are displayed. Scale bar = 100 μm. **G**–**H** Transwell migration and invasion assays demonstrating that PLAAT2 knockdown markedly suppressed cell motility. Representative images (upper panels) and (**K**-**L**) quantification (lower panels) are provided. Scale bar = 200 μm. **I**–**J** Wound-healing assay showing delayed gap closure in siPLAAT2-transfected cells compared with NC. Representative fields at 0 and 24 h and (**M**–**N**) corresponding quantitative analyses are presented. Scale bar = 200 μm. (*$P < 0.05$; **$P < 0.01$; ***$P < 0.001$,****$P < 0.0001$)

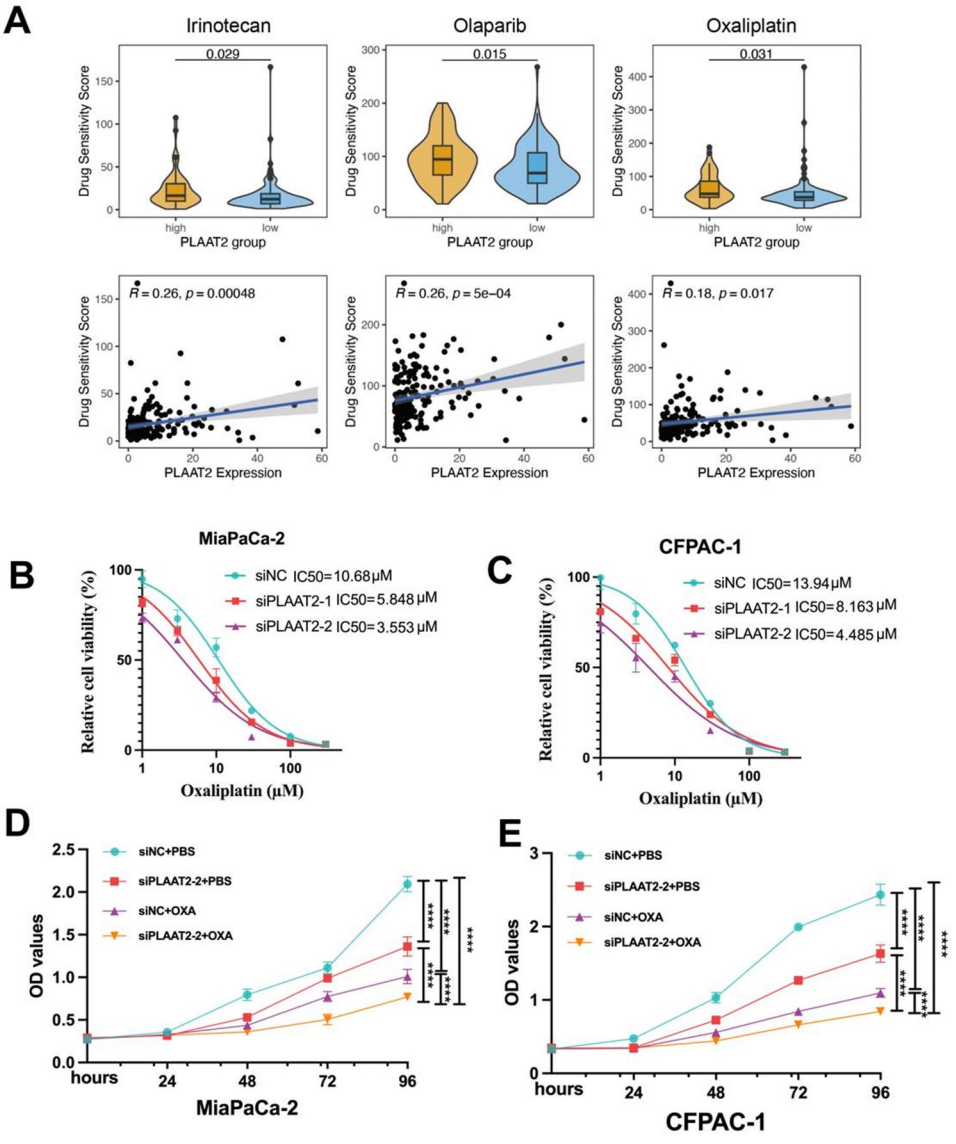



**Fig. 12** PLAAT2 expression is associated with chemotherapeutic response and its silencing enhances oxaliplatin sensitivity in PC cells. **A** Predicted drug response to irinotecan, olaparib and oxaliplatin in the TCGA-PAAD cohort. Upper panels: violin/box plots comparing oncoPredict-derived drug response scores between PLAAT2-high and PLAAT2-low groups. Lower panels: scatter plots showing the correlation between PLAAT2 mRNA expression and drug response scores for each agent; lines represent linear regression fits, and R and P values are indicated. **B**, **C** Dose–response curves for oxaliplatin in MiaPaCa-2 (B) and CFPAC-1 (C) cells transfected with negative control siRNA (siNC) or two independent PLAAT2 siRNAs (siPLAAT2-1 and siPLAAT2-2). Cell viability was measured by CCK-8 assay after 72 h of drug exposure, and $IC_{50}$ values are shown in the insets. **D**, **E** Time-course CCK-8 assays evaluating the combined effects of PLAAT2 knockdown and oxaliplatin on cell proliferation in MiaPaCa-2 (D) and CFPAC-1 (E) cells. Cells were transfected with siNC or siPLAAT2-2 and treated with PBS or oxaliplatin (OXA) as indicated; OD values were recorded at 0, 24, 48, 72 and 96 h. Data are presented as mean ± SD from three independent experiments ($n = 3$). $IC_{50}$ values in (B, C) were calculated by nonlinear regression using a variable-slope dose–response model in GraphPad Prism

targeting specific PLAAT2-dependent lipid species will be needed to clarify these relationships.

On the clinical side, we derived an 11-gene PLAAT2-associated prognostic signature that stratified patients into distinct risk groups with significantly different survival outcomes in both the TCGA and external GEO cohorts. Although PLAAT2 itself was not retained in the final LASSO model, the selected genes can be viewed as capturing a PLAAT2-related transcriptional programme, which may better reflect the downstream consequences of PLAAT2 dysregulation than PLAAT2 expression alone. Importantly, high-risk patients defined by this signature exhibited unfavourable predicted responses to irinotecan, olaparib and oxaliplatin. While these drug-sensitivity estimates are based on in silico modelling, they suggest that PLAAT2-associated transcriptional features may be informative for therapeutic stratification. Validation of this signature in prospective, treatment-annotated cohorts will be necessary before it can be considered for clinical decision-making.

In vitro, we confirmed that PLAAT2 is overexpressed in multiple PC cell lines and that its knockdown inhibits proliferation, migration and invasion, which is consistent with an oncogenic function. Moreover, silencing PLAAT2 significantly enhanced the growth-inhibitory effect of oxaliplatin in MiaPaCa-2 and CFPAC-1 cells, as evidenced by leftward shifts in dose–response curves and reduced $IC_{50}$ values, as well as more pronounced suppression of cell viability over time. These findings are in agreement with our bioinformatic prediction that PLAAT2-high tumours may be less sensitive to several commonly used agents, and they highlight the possibility that targeting PLAAT2 could potentiate the efficacy of oxaliplatin-based chemotherapy. Future studies incorporating apoptosis, DNA-damage and ferroptosis assays may help elucidate how PLAAT2 modulation influences oxaliplatin response at the mechanistic level.

Several limitations of this study should be acknowledged. First, the bulk of our bioinformatic analyses were retrospective and based on publicly available datasets, which may be subject to selection bias and batch effects. Second, although we expanded our institutional validation to 15 paired tumour and adjacent tissues, the cohort size remains modest and from a single centre, limiting the generalizability of the clinicopathological correlations. Third, our functional validation relied on cell-based assays; in vivo models, such as patient-derived xenografts or genetically engineered mice, will be required to confirm the role of PLAAT2 in tumour growth, metastasis and treatment response. Fourth, while our enrichment analyses point to lipid metabolic pathways and immune alterations, the precise lipid species, signalling cascades and immune-cell subsets directly regulated by PLAAT2 remain to be defined. Finally, the drug-sensitivity analyses for irinotecan and olaparib were based on computational prediction rather than direct pharmacological testing, and even for oxaliplatin, only a limited range of in vitro conditions was examined. These issues underscore the need for further mechanistic and translational studies before PLAAT2 or its associated signature can be implemented in clinical practice.

## Conclusion

In summary, our study integrates multi-omics analyses and experimental evidence to support an oncogenic role of PLAAT2 in PC. PLAAT2 is overexpressed in PC tissues, associates with adverse clinicopathological features and poorer survival, and is linked to distinct metabolic, immune and mutational characteristics. A PLAAT2-related multigene signature provides additional prognostic information and suggests potential differences in chemotherapeutic response, while in vitro experiments indicate that PLAAT2 depletion can enhance the sensitivity of PC cells to oxaliplatin. Although constrained by retrospective design, a relatively small validation cohort and the lack of in vivo mechanistic interrogation, these findings collectively highlight PLAAT2 and its downstream transcriptional programme as candidate biomarkers and potential therapeutic entry points in PC. Further studies combining detailed mechanistic investigations with prospective clinical validation will be essential to determine how PLAAT2-directed strategies might be incorporated into precision treatment approaches for this lethal disease.

## Supplementary Information

The online version contains supplementary material available at https://doi.org/10.1186/s12885-025-15481-2.

Supplementary Material 1.

Supplementary Material 2.

Supplementary Material 3.

### Authors' contributions

Conceptualization and study design: Qingsong Guo, Yuhua Lu; Funding acquisition: Qingsong Guo; Supervision and experimental support: Yuhua Lu (provided laboratory platform and technical support); Bioinformatics analysis: Qiyang Chen; Experimental validation (in vitro): Qiyang Chen; assistance from Ting Liang, Chenhao Wu; Data curation and statistical analysis: Qiyang Chen, Ting Liang, Jingjing Lu, Xiaohong Li; Clinical resources, patient recruitment, and sample collection: Jian Wan; Manuscript drafting: Qiyang Chen; Critical revision of the manuscript: Xiaohong Li, Jingjing Lu, Qingsong Guo, Yuhua Lu.

### Funding

This work was financially supported by the Science and technology project of Nantong City (JC2024080).

### Data availability

All data utilized and analyzed in this study are accessible from the TCGA database (https://portal.gdc.cancer.gov/) and the GEO database ( [https://www.ncbi.nlm.nih.gov/geo/](https://www.ncbi.nlm.nih.gov/geo/) ).

## Declarations

### Ethics approval and consent to participate

The use of human PC tissue samples in this study was approved by the Ethics Committee of the Affiliated Hospital of Nantong University (Approval No. 2025-K195). Written informed consent was obtained from all participants prior to surgery. This study was conducted in accordance with the Declaration of Helsinki.

### Consent for publication

Not applicable.

### Competing interests

The authors declare no competing interests.

### Author details

[1]Department of Hepatobiliary and Pancreatic Surgery, Affiliated Hospital of Nantong University, Medical School of Nantong University, Nantong 226001, PR China
[2]Department of Pathology, Affiliated Hospital of Nantong University, Medical School of Nantong University, Nantong 226001, China
[3]Research Center of Clinical Medicine, Affiliated Hospital of Nantong University, Nantong, Jiangsu Province 226001, PR China

Received: 2 September 2025 / Accepted: 16 December 2025
Published online: 20 December 2025

### References

1. Siegel RL, Giaquinto AN, Jemal A. Cancer statistics, 2024. CA Cancer J Clin. 2024;74(1):12–49.
2. McGuigan A, et al. Pancreatic cancer: A review of clinical diagnosis, epidemiology, treatment and outcomes. World J Gastroenterol. 2018;24(43):4846–61.
3. Kleeff J, et al. Pancreatic cancer. Nat Rev Dis Primers. 2016;2:16022.
4. Bailey P, et al. Genomic analyses identify molecular subtypes of pancreatic cancer. Nature. 2016;531(7592):47–52.
5. Waddell N, et al. Whole genomes redefine the mutational landscape of pancreatic cancer. Nature. 2015;518(7540):495–501.
6. Biankin AV, et al. Pancreatic cancer genomes reveal aberrations in axon guidance pathway genes. Nature. 2012;491(7424):399–405.
7. Wong HH, Lemoine NR. Pancreatic cancer: molecular pathogenesis and new therapeutic targets. Nat Rev Gastroenterol Hepatol. 2009;6(7):412–22.
8. Pavlova NN, Thompson CB. The Emerg Hallm Cancer Metabolism Cell Metab. 2016;23(1):27–47.
9. Vander Heiden MG, DeBerardinis RJ. Understanding the intersections between metabolism and cancer biology. Cell. 2017;168(4):657–69.
10. Hanahan D. Hallmarks of cancer: new dimensions. Cancer Discov. 2022;12(1):31–46.
11. Currie E, et al. Cellular fatty acid metabolism and cancer. Cell Metab. 2013;18(2):153–61.
12. Beloribi-Djefaflia S, Vasseur S, Guillaumond F. Lipid metabolic reprogramming in cancer cells. Oncogenesis. 2016;5(1):e189.
13. Röhrig F, Schulze A. The multifaceted roles of fatty acid synthesis in cancer. Nat Rev Cancer. 2016;16(11):732–49.
14. Yue S, et al. Cholesteryl ester accumulation induced by PTEN loss and PI3K/AKT activation underlies human prostate cancer aggressiveness. Cell Metab. 2014;19(3):393–406.
15. Uyama T, et al. Generation of N-acylphosphatidylethanolamine by members of the phospholipase A/acyltransferase (PLA/AT) family. J Biol Chem. 2012;287(38):31905–19.
16. Uyama T, et al. Regulation of peroxisomal lipid metabolism by catalytic activity of tumor suppressor H-rev107. J Biol Chem. 2012;287(4):2706–18.
17. Shinohara N, et al. Enzymological analysis of the tumor suppressor A-C1 reveals a novel group of phospholipid-metabolizing enzymes. J Lipid Res. 2011;52(11):1927–35.
18. Mardian EB, Bradley RM, Duncan RE. The HRASLS (PLA/AT) subfamily of enzymes. J Biomed Sci. 2015;22:99.
19. Ling Y, et al. HRASLS2 promotes the growth and glycolysis of pancreatic cancer by enhancing the stability of ASPH. Naunyn Schmiedebergs Arch Pharmacol. 2025. https://doi.org/10.1007/s00210-025-04522-z.
20. Binnewies M, et al. Understanding the tumor immune microenvironment (TIME) for effective therapy. Nat Med. 2018;24(5):541–50.
21. Hegde PS, Chen DS. Top 10 challenges in cancer immunotherapy. Immunity. 2020;52(1):17–35.
22. Zhang Y, et al. Myeloid cells are required for PD-1/PD-L1 checkpoint activation and the establishment of an immunosuppressive environment in pancreatic cancer. Gut. 2017;66(1):124–36.
23. Livak KJ, Schmittgen TD. Analysis of relative gene expression data using real-time quantitative PCR and the 2(-Delta delta C(T)) method. Methods. 2001;25(4):402–8.
24. Kramer N, et al. In vitro cell migration and invasion assays. Mutat Res. 2013;752(1):10–24.
25. Liang CC, Park AY, Guan JL. Vitro scratch assay: a convenient and inexpensive method for analysis of cell migration in vitro. Nat Protoc. 2007;2(2):329–33.
26. Davis S, Meltzer PS. GEOquery: a Bridge between the gene expression omnibus (GEO) and bioconductor. Bioinformatics. 2007;23(14):1846–7.
27. Love MI, Huber W, Anders S. Moderated Estimation of fold change and dispersion for RNA-seq data with DESeq2. Genome Biol. 2014;15(12):550.
28. Xu S, et al. Using clusterprofiler to characterize multiomics data. Nat Protoc. 2024;19(11):3292–320.
29. Yu G, et al. ClusterProfiler: an R package for comparing biological themes among gene clusters. Omics. 2012;16(5):284–7.
30. Newman AM, et al. Robust enumeration of cell subsets from tissue expression profiles. Nat Methods. 2015;12(5):453–7.
31. Friedman J, Hastie T, Tibshirani R. Regularization paths for generalized linear models via coordinate descent. J Stat Softw. 2010;33(1):1–22.
32. Yoshihara K, et al. Inferring tumour purity and stromal and immune cell admixture from expression data. Nat Commun. 2013;4:2612.
33. Maeser D, Gruener RF, Huang RS. OncoPredict: an R package for predicting in vivo or cancer patient drug response and biomarkers from cell line screening data. Brief Bioinform. 2021;22(6):bbab260. https://doi.org/10.1093/bib/bbab260.
34. Waters AM, Der CJ. KRAS: the critical driver and therapeutic target for pancreatic cancer. Cold Spring Harb Perspect Med. 2018;8(9):a031435. https://doi.org/10.1101/cshperspect.a031435.

## Publisher's Note

Springer Nature remains neutral with regard to jurisdictional claims in published maps and institutional affiliations.